Stochastic waves in a Brusselator model with nonlocal interaction

Tommaso Biancalani,[*] Tobias Galla,[†] and Alan J. McKane[‡]
Theoretical Physics Division, School of Physics and Astronomy, University of Manchester, Manchester M13 9PL, United Kingdom
(Received 4 April 2011; published 5 August 2011)

We show that intrinsic noise can induce spatiotemporal phenomena such as Turing patterns and traveling waves in a Brusselator model with nonlocal interaction terms. In order to predict and to characterize these stochastic waves we analyze the nonlocal model using a system-size expansion. The resulting theory is used to calculate the power spectra of the stochastic waves analytically and the outcome is tested successfully against simulations. We discuss the possibility that nonlocal models in other areas, such as epidemic spread or social dynamics, may contain similar stochastically induced patterns.

DOI: 10.1103/PhysRevE.84.026201 PACS number(s): 89.75.Kd, 05.40.−a, 82.40.Ck, 02.50.Ey

I. INTRODUCTION

The underlying idea of the theory of complex systems is that complex patterns or structures can be generated from simple models; one of the key papers leading to this insight was the classic paper of Turing [1] on what are now known as reaction-diffusion equations. Most of the theoretical studies of pattern formation have followed Turing and used partial differential equations (PDEs) to specify the model describing the system [2]. However, there is a potential problem with this approach: The parameter range for which the patterns exist in the model can be very restricted, in contrast with what is seen in real systems. For instance, to observe Turing patterns in simple reaction-diffusion systems described by PDEs requires that the diffusivities of the species be of different orders [2,3]. The limited range of parameters for which patterns are seen could be attributed to the simplicity of the model chosen to describe the process; however, for systems with an underlying molecular basis another explanation has recently been put forward in Refs. [4–6]. Those authors have observed that Turing-like patterns exist for a much greater range of parameter values if the discrete nature of the molecules comprising the system is taken into account. The resulting patterns are sometimes referred to as stochastic Turing patterns [5] or quasi-Turing patterns [7] and they may be analyzed using the theory of stochastic processes, which is appropriate given the noise is created as a consequence of the discreteness of the system.

In this paper we investigate a model that shows not only Turing and stochastic Turing patterns, but also traveling waves and stochastic traveling waves (referred to as stochastic waves in the following), the latter having the same relation to traveling waves that Turing patterns have to stochastic Turing patterns. One interesting aspect of stochastic waves is that they can clearly be seen in computer simulations of the model. In contrast, while there is unambiguous evidence for the existence of stochastic Turing patterns from, for instance, the form of the power spectrum of the fluctuations, direct visual evidence is less clear due to the noisy nature of the patterns. The model we study is a Brusselator with a nonlocal interaction term; this choice is largely made on the grounds that the model is simple and so allows the effect to be clearly demonstrated. The nonlocality seems to be an important ingredient in finding stochastic waves, similar to the observation that traveling waves disappear in deterministic models when interactions are made more local [8]. Traveling waves have been observed in chemical reaction systems in [9–11] and also in other types of population-based systems [12–15].

The description of patterns through an analysis of PDEs of the reaction-diffusion type is well developed [2], but the analogous stochastic systems have received very little attention. The common starting point of the work that has been carried out [4–6] has been the master equation (continuous-time Markov chain), although the details of the techniques used to analyze this equation have differed. However, the whole idea of stochastic patterns as well as the methods that may be used to analyze them follows from the idea of stochastic cycles, or quasicycles, and their detailed study over the past few years. Since the essential idea behind stochastic patterns can be clarified with reference to the well-studied mechanism behind stochastic cycles, we turn to their description.

The context in which stochastic cycles appear is in the relation between stochastic individual-based models and the corresponding deterministic descriptions of their dynamics. Interacting many-particle systems are typically defined by a set of stochastic rules at the microscopic level. Such systems are common in chemistry and in biology [16], but they are also used to model stochastic dynamics in epidemiology [17,18], in population dynamics [19,20], and in the social sciences [21]. Frequently, in formulating descriptions of these systems intrinsic noise, due to the discrete nature of the constituents, is treated as a negligible perturbation to the dominant deterministic dynamics. It has been known for many years that neglecting such fluctuations is not always justified; on the contrary, intrinsic noise can fundamentally change the temporal evolution of these systems. The activity in this area over the past few years is due to the realization that a method imported from statistical physics—the van Kampen system-size expansion [16]—can be used to *quantitatively* understand the deviations to the deterministic dynamics caused by these stochastic effects. Effectively, one uses some measure of the inverse system size, for instance, its inverse volume V^{-1}, as a perturbation parameter to investigate the stochastic dynamics.

[*]tommaso.biancalani@postgraduate.manchester.ac.uk
[†]tobias.galla@manchester.ac.uk
[‡]alan.mckane@manchester.ac.uk

 ©2011 American Physical Society

If truncated after the lowest order, the system-size expansion provides a systematic path from stochastic microscopic interacting-particle models to a deterministic description in terms of differential equations. This truncation effectively corresponds to taking the thermodynamic limit, i.e., to considering the limiting case of infinite systems. If carried out to next-to-leading order the system-size expansion can successfully characterize stochastic effects in the limit of large but finite systems. Of particular interest is the case where the deterministic model has a stable fixed point, which is a spiral, so that perturbations away from the fixed point decay in an oscillatory manner. The effect of the stochasticity is to excite this decaying mode and create sustained oscillations, which have an amplitude larger than might naively be expected—stochastic amplification [19]. These are the stochastic cycles.

In this description of stochastic cycles no mention has been made of the spatial degrees of freedom and indeed most of the studies of stochastic cycles have been confined to well-mixed systems where spatial effects are ignored. However, in a similar way, intrinsic fluctuations can excite more complicated spatiotemporal modes in spatially extended systems, as seen, for example, in a predator-prey model of the Volterra type [22]. In this spatially extended model the intrinsic noise leads to spatially uniform temporal oscillations, i.e., at a zero wave number. Stochastic Turing patterns, just like stochastic cycles, are triggered by internal fluctuations, but they occur at a nonzero wave number. To date they have been found in a spatial version of the Levin-Segel predator-prey model [4], in the spatial Brusselator model [5], and in a model of embryonic patterning [6]. What does not change is the ability of the system-size expansion to accurately predict the features of the excitations.

The main purpose of the present paper is to show that in addition to uniform spatial oscillations and time-independent Turing patterns, intrinsic noise can also trigger traveling waves, i.e., phenomena that are both spatial and temporal simultaneously. To show that such effects may occur we study a variation of the Brusselator model with a nonlocal interaction term, mediated by an exponential kernel in space. We believe that the existence of stochastic traveling waves is widespread and we choose the Brusselator model because it is probably the most widely used model to illustrate such phenomena and so is familiar to a wide number of researchers in the field. A disadvantage is that nonlocal interactions that seem to be required to see the effect are less easy to motivate in a chemical model such as the Brusselator, but we believe that this is outweighed by the advantage of using a simple model to illustrate the idea. So while several physical mechanisms for nonlocal interactions are given in Ref. [8], and in biological and social systems such effects are far easier to describe and motivate, our desire in this paper to avoid specific mechanisms and extraneous details leads us to formulate the nonlocal interaction in a simple and generic way.

We show that the presence of such a nonlocal term promotes traveling waves and that stochasticity can bring about stochastic traveling waves in situations where the deterministic system has a stable uniform fixed point. All this is carried out analytically through use of the system-size expansion—extended to deal with the nonlocal interaction—and checked numerically using the Gillespie algorithm [23,24].

The remainder of the paper is structured as follows. In Sec. II we introduce the model and discuss its behavior on the deterministic level. In Sec. III we carry out a detailed analysis of the stochastic dynamics by means of an expansion in the inverse system size. Section IV contains our main results, including an analytical characterization of stochastic waves and confirmation through numerical simulations. Our findings are summarized in Sec. V, where we also discuss possible future lines of research. Two appendixes contain mathematical details: the first a summary of the conditions under which Turing and wave instabilities occur and the second aspects of the calculations and results from the system-size expansion.

II. MODEL DEFINITION

The stochastic model is defined as a collection of uniform cells, indexed by i, each of which has volume V. For convenience these can be thought of as cubes in three dimensions, but other regular shapes in other dimensions can also be considered. In fact, since our main aim here is to illustrate the idea of stochastic waves and their characterization, our results will largely apply to a one-dimensional system, i.e., a chain of cells. Simulations are then less time consuming, but the model still exhibits all features we are interested in studying. Generalization of the analytic results to higher-dimensional models is straightforward. Unlike previous work [22], we will assume that the number of cells is infinite, that is, the underlying space is of infinite extent. This avoids technical complications when nonlocal interactions are present.

In every cell molecules of two species X and Y interact through the reactions of the Brusselator model [25]:

$$\begin{aligned} \emptyset_i &\xrightarrow{a} X_i, \\ X_i &\xrightarrow{b} Y_i, \\ 2X_i + Y_i &\xrightarrow{c} 3X_i, \\ X_i &\xrightarrow{d} \emptyset_i. \end{aligned} \tag{1}$$

The rates at which the reactions occur are denoted by a, b, c, and d and X_i and Y_i are molecules that are in cell i at the time the reaction occurs. The third reaction may occur between an X molecule in cell i and a Y molecule in any other cell (with rates depending on the distance between the two cells), but the effect is to reduce the number of Y molecules in cell i by 1. This constitutes the nonlocal interaction; other choices are possible, but this was made on grounds of simplicity. The notation used to describe the chemical types and the rates in the Brusselator model in the literature is not standard, but we follow most closely Ref. [26]. The number of X and Y molecules in cell i will be denoted by n_i and m_i, respectively. We will also use $\mathbf{n}$ and $\mathbf{m}$ to represent the spatial vectors with components n_i and m_i, respectively.

The transition rate from the state $(\mathbf{n},\mathbf{m})$ to the state $(\mathbf{n}',\mathbf{m}')$ will be denoted by $T(\mathbf{n}',\mathbf{m}'|\mathbf{n},\mathbf{m})$, but to lighten the notation we will only list the variables that have changed in a given reaction. These functions are found by invoking mass action:

$$\begin{aligned} T_1(n_i+1,m_i|n_i,m_i) &= a, \\ T_2(n_i-1,m_i+1|n_i,m_i) &= b\,\frac{n_i}{V}, \end{aligned}$$

$$T_3(n_i+1,m_i-1|n_i,m_i) = c\,\frac{{n_i}^2}{V^2}\,\Lambda\sum_{j=-\infty}^{\infty} e^{-\sigma|i-j|}\,\frac{m_j}{V}, \quad (2)$$

$$T_4(n_i-1,m_i|n_i,m_i) = d\,\frac{n_i}{V},$$

where the subscripts on the rates refer to the four reactions in Eq. (1). These transition rates are as in the usual Brusselator model [26], except for the third, which has the nonlocal character mentioned earlier. We stress again that it is the influence of the Y molecule in cell j that causes the reaction, but that the effect is in cell i, which is a distance $|i-j|$ away. The effect is to increase the number of X molecules in cell i by one and to decrease the number of Y molecules in cell i by one. The form of interaction was taken to be exponential because this is a frequent choice, but once again on grounds of simplicity. The constant σ expresses the range of the interaction and Λ is a normalization constant whose choice will be discussed later. As a technical aside, the third transition rate should also have a factor of $\theta(m_i)$—the Heaviside step function—present to prevent the number of Y molecules in cell i from becoming negative, but given we will be looking at a regime far from $m_i = 0$, this condition is irrelevant.

In addition to the reactions given in Eq. (1), migration reactions, which describe molecular diffusion from one cell to another, have to be specified. For a given cell i, molecules of the two species X and Y may diffuse into or diffuse out of a neighboring cell j:

$$X_i \xrightarrow{\alpha} X_j, \quad X_j \xrightarrow{\alpha} X_i,$$
$$Y_i \xrightarrow{\beta} Y_j, \quad Y_j \xrightarrow{\beta} Y_i. \quad (3)$$

These reactions have transition rates given by

$$T_5(n_i-1,n_j+1|n_i,n_j) = \alpha\,\frac{n_i}{Vz},$$
$$T_6(n_i+1,n_j-1|n_i,n_j) = \alpha\,\frac{n_j}{Vz},$$
$$T_7(m_i-1,m_j+1|m_i,m_j) = \beta\,\frac{m_i}{Vz}, \quad (4)$$
$$T_8(m_i+1,m_j-1|m_i,m_j) = \beta\,\frac{m_j}{Vz}.$$

Here z is the number of nearest neighbors of a cell and the index j denotes a nearest neighbor of cell i. For the one-dimensional model $z = 2$ and $j \in \{i-1, i+1\}$. It is also worth remarking that we have not imposed a fixed limit on the number of molecules permitted in a cell (in contrast with some previous work [5,22]; this is reflected in the fact we use the inverse volume V^{-1} rather than the inverse total number of molecules as the expansion parameter).

Since we have assumed that the transition rates depend only on the current state of the system, the stochastic process is Markovian and so the probability distribution for the system being in state $(\mathbf{n},\mathbf{m})$ at time t, $P_{\mathbf{n},\mathbf{m}}(t)$, satisfies the master equation [16]

$$\frac{d}{dt}P_{\mathbf{n},\mathbf{m}}(t) = \sum_{(\mathbf{n}',\mathbf{m}')\neq(\mathbf{n},\mathbf{m})} [T(\mathbf{n},\mathbf{m}|\mathbf{n}',\mathbf{m}')P_{\mathbf{n}',\mathbf{m}'}(t) - T(\mathbf{n}',\mathbf{m}'|\mathbf{n},\mathbf{m})P_{\mathbf{n},\mathbf{m}}(t)]. \quad (5)$$

In what follows we will write discrete variables as subscripts and continuous variables as arguments of functions [such as in $P_{\mathbf{n},\mathbf{m}}(t)$]. The sole exception is for the transition rates $T(\mathbf{n}',\mathbf{m}'|\mathbf{n},\mathbf{m})$, where for the sake of clarity we have written the discrete variables as arguments of the function T.

We will discuss the analysis of the master equation (5) using the system-size expansion in Sec. III. For the rest of this section we will obtain directly the deterministic equation that holds in the limit $V \to \infty$, without using the system-size expansion, and then study the stability of the homogeneous state.

We begin by defining the concentrations of the X and Y molecules in cell i in the infinite volume limit by

$$\phi_i(t) = \lim_{V\to\infty}\frac{\langle n_i\rangle}{V}, \quad \psi_i(t) = \lim_{V\to\infty}\frac{\langle m_i\rangle}{V}, \quad (6)$$

where $\langle\ \rangle$ is the mean with respect to the probability distribution $P_{\mathbf{n},\mathbf{m}}(t)$. Multiplying Eq. (5) by n_i and m_i, respectively, and using the fact that in the deterministic limit the probability distribution is a delta function so that $\langle n_i^\ell\rangle = \langle n_i\rangle^\ell$, etc., one finds the following ordinary differential equations:

$$\frac{d}{d\tau}\phi_i = a - (b+d)\phi_i + c\phi_i^2\Lambda\sum_{j=-\infty}^{\infty} e^{-\sigma|j|}\psi_{i-j} + \alpha\Delta\phi_i,$$
$$\frac{d}{d\tau}\psi_i = b\phi_i - c\phi_i^2\Lambda\sum_{j=-\infty}^{\infty} e^{-\sigma|j|}\psi_{i-j} + \beta\Delta\psi_i, \quad (7)$$

where $\tau = t/V$ is a rescaled time and $\Delta f_i = f_{i+1} - 2f_i + f_{i-1}$ is the discrete one-dimensional Laplacian.

We choose the normalization constant Λ so as to satisfy

$$\Lambda\sum_{j=-\infty}^{\infty} e^{-\sigma|j|} = 1. \quad (8)$$

By doing so, the deterministic equations (7) have the homogeneous solution

$$\phi_i = \phi^* = \frac{a}{d}, \quad \psi_i = \psi^* = \frac{bd}{ac}, \quad (9)$$

which are the same as those of the conventional Brusselator model (obtained from our model by replacing the nonlocal interaction by a local term). The expression for Λ can be summed to yield

$$\Lambda = \frac{e^\sigma - 1}{e^\sigma + 1}. \quad (10)$$

Equations (7) are a set of reaction-diffusion equations of the type usually defining the starting point for finding Turing patterns. The analysis starts by examining if the homogeneous solution in Eq. (9) is unstable to spatially inhomogeneous small perturbations. To do this we introduce small perturbations

$$\delta\phi_i(t) = \phi_i(t) - \phi^*, \quad \delta\psi_i(t) = \psi_i(t) - \psi^* \quad (11)$$

into the deterministic equations (7) and keep only linear terms in $\delta\phi_i(t)$ and $\delta\psi_i(t)$. This gives

$$\frac{d}{d\tau}\delta\phi_i = -(b+d)\delta\phi_i + c\phi^{*2}\Lambda\sum_{j=-\infty}^{\infty} e^{-\sigma|j|}\delta\psi_{i-j} + 2c\phi^*\psi^*\delta\phi_i + \alpha\Delta\delta\phi_i, \quad (12)$$

$$\frac{d}{d\tau}\delta\psi_i = b\delta\phi_i - c\phi^{*2}\Lambda \sum_{j=-\infty}^{\infty} e^{-\sigma|j|}\delta\psi_{i-j} - 2c\phi^*\psi^*\delta\phi_i + \beta\Delta\delta\psi_i. \quad (13)$$

The structure of these equations makes it clear that they will simplify considerably if we go over to a Fourier representation. We therefore introduce the spatial Fourier transform for the infinite discrete system of cells:

$$\tilde{f}(k) = \sum_{j=-\infty}^{\infty} e^{-ijk} f_j, \quad f_j = \frac{1}{2\pi}\int_0^{2\pi} dk\, e^{ikj}\tilde{f}(k). \quad (14)$$

Note that k is a continuous variable that takes values in the first Brillouin zone $[0,2\pi]$. Fourier transforming Eqs. (12) and (13) gives

$$\frac{\partial}{\partial\tau}\delta\tilde{\phi} = -(b+d)\delta\tilde{\phi} + c\phi^{*2}\Lambda\tilde{e}(k)\delta\tilde{\psi} + 2c\phi^*\psi^*\delta\tilde{\phi} + \alpha\tilde{\Delta}\delta\tilde{\phi}, \quad (15)$$

$$\frac{\partial}{\partial\tau}\delta\tilde{\psi} = b\delta\tilde{\phi} - c\phi^{*2}\Lambda\tilde{e}(k)\delta\tilde{\psi} - 2c\phi^*\psi^*\delta\tilde{\phi} + \beta\tilde{\Delta}\delta\tilde{\psi}, \quad (16)$$

where $\delta\tilde{\phi} = \delta\tilde{\phi}(k,\tau)$ and similarly for $\delta\tilde{\psi}$. The two functions $\tilde{e}(k)$ and $\tilde{\Delta} \equiv \tilde{\Delta}(k)$ are, respectively, the Fourier transform of the exponential function and of the Laplacian, i.e.,

$$\widetilde{\Delta f}(k) = \sum_{j=-\infty}^{\infty} e^{-ikj}(f_{j+1} - 2f_j + f_{j-1}) = 2\left[\cos(k) - 1\right]\tilde{f}(k) \Rightarrow \tilde{\Delta} \equiv 2\left[\cos(k) - 1\right],$$
$$\tilde{e}(k) = \sum_{j=-\infty}^{\infty} e^{-\sigma|j|}e^{-ikj} = \frac{\sinh(\sigma)}{\cosh(\sigma) - \cos(k)}. \quad (17)$$

The system in Eqs. (15) and (16) may be written in a more compact form

$$\frac{\partial}{\partial\tau}\begin{pmatrix}\delta\tilde{\phi}\\ \delta\tilde{\psi}\end{pmatrix} = \mathcal{J}^*(k)\cdot\begin{pmatrix}\delta\tilde{\phi}\\ \delta\tilde{\psi}\end{pmatrix}, \quad (18)$$

where

$$\mathcal{J}^*(k) = \begin{pmatrix} -(b+d) + 2c\phi^*\psi^* + \alpha\tilde{\Delta} & c\Lambda\phi^{*2}\tilde{e}(k) \\ b - 2c\phi^*\psi^* & -c\Lambda\phi^{*2}\tilde{e}(k) + \beta\tilde{\Delta}\end{pmatrix}. \quad (19)$$

The eigenvalues of the Jacobian matrix Eq. (19), $\lambda_1(k)$ and $\lambda_2(k)$, yield information about whether perturbing the homogeneous solution leads to pattern formation. If both λ_1 and λ_2 have a negative real part (i.e., $\mathrm{Re}[\lambda_i(k)] < 0\ \forall k$, $i = 1,2$), the homogeneous state is stable: Every perturbation will eventually die out and no pattern will develop. If, on the other hand, there is an eigenvalue at a nonzero k with a positive real part, then a spatially modulated instability occurs: A perturbation will grow in magnitude, taking the system from the homogeneous state to one with the wave number defined by k. This growth will eventually be saturated by the nonlinear terms leading to a pattern of characteristic wave number k.

This linear analysis of the homogeneous state is also able to determine whether the resulting pattern is steady or oscillatory by looking at the imaginary part of the eigenvalues $\omega_i \equiv \mathrm{Im}[\lambda_i]$. Steady patterns correspond to $\mathrm{Im}[\lambda_i(k)] = 0$ for all unstable modes k, the case in which the instability is called a Turing instability. When $\mathrm{Im}[\lambda_i(k)] \neq 0$ for an unstable mode at a nonzero k, the system is said to undergo a wave instability as the resulting pattern will consist of traveling waves [2].

When multiple instabilities occur simultaneously, say, of the Turing type for some k_1 and the wave type for some k_2, it becomes harder to predict if the final pattern will be steady or oscillatory. However, for model parameters sufficiently close to the region in which the homogeneous state is stable, only a single instability occurs. We will therefore study the instabilities at the border of the stable region, saying that there is a Turing instability (wave instability) when the instability near the border is of the Turing type (wave type). The criteria we use to determine the stability boundaries are discussed in Appendix A.

The above analysis applied to Eq. (19) is discussed in Sec. IV. However, as explained in the Introduction, we wish to go beyond this deterministic approximation and examine patterns that emerge from stochastic effects that are a consequence of the underlying discreteness of the system. We therefore now go on to discuss the stochastic analysis of the model before collecting together results of the determinstic and stochastic regimes in Sec. IV.

III. STOCHASTIC ANALYSIS

The analysis of the model, without making the deterministic approximation, begins by writing down the master equation (5) in a form that is more amenable to application of the system-size expansion. This is done by introducing step operators [16]

$$\epsilon^{\pm}_{X,i} f(\mathbf{n},\mathbf{m}) = f(\ldots,n_i \pm 1,\ldots,\mathbf{m}),$$
$$\epsilon^{\pm}_{Y,i} f(\mathbf{n},\mathbf{m}) = f(\mathbf{n},\ldots,m_i \pm 1,\ldots). \quad (20)$$

For example, the term in the master equation that involves the first reaction in Eq. (1), and thus corresponds to the function T_1 in Eq. (2), would be given by

$$\sum_i (\epsilon^-_{X,i} - 1)\, T_1(n_i+1, m_i | n_i, m_i) P_{\mathbf{n},\mathbf{m}}(t) = \sum_i (\epsilon^-_{X,i} - 1)\, a\, P_{\mathbf{n},\mathbf{m}}(t). \quad (21)$$

The master equation rewritten in this way, with all eight terms present, is given by Eq. (B1).

We will now carry out the system-size expansion. It is important to realize that, for our model, this is an expansion in powers of $V^{-1/2}$, where V is the volume per cell. The expansion therefore captures stochastic effects at large, but finite cell volumes. This limit should not be confused with the limit of an infinite number of cells. When we use the term "system-size expansion" we always refer to an expansion in the size (volume) of a single cell. Even if the volume per cell is finite, the total number of molecules in the system (summed

over all cells) may well be infinite if the system is composed of an infinite number of cells.

The system-size expansion itself involves making the time-dependent change of variables $(\mathbf{n},\mathbf{m}) \mapsto (\boldsymbol{\xi},\boldsymbol{\eta})$:

$$\mathbf{n} \mapsto V\boldsymbol{\phi}(t) + \sqrt{V}\boldsymbol{\xi}, \quad \mathbf{m} \mapsto V\boldsymbol{\psi}(t) + \sqrt{V}\boldsymbol{\eta}, \tag{22}$$

where $\boldsymbol{\phi}(t)$ and $\boldsymbol{\psi}(t)$ are two time-dependent vectors defined by Eq. (6), each of these vectors having as many components as there are different cells in the system. From the leading-order term in the expansion one finds that these quantities satisfy the deterministic equation (7).

We now change the degrees of freedom of the stochastic system to $\boldsymbol{\xi}$ and $\boldsymbol{\eta}$ and consider the probability distribution in terms of these variables as

$$\Pi(\boldsymbol{\xi},\boldsymbol{\eta},t) = P_{\mathbf{n},\mathbf{m}}(t). \tag{23}$$

The left-hand side of the master equation (5) has the form [16]

$$\frac{dP}{dt} = \partial_t \Pi - \sqrt{V}\nabla_{\xi}\Pi \cdot \partial_t\boldsymbol{\phi} - \sqrt{V}\nabla_{\eta}\Pi \cdot \partial_t\boldsymbol{\psi}, \tag{24}$$

where $\partial_t = \partial/\partial t$.

To determine the nature of the expansion of the right-hand side of the master equation we begin with the form of Eq. (B1) given in terms of the step operators. This is because the step operators have a natural expansion in $V^{-1/2}$ given in Eq. (B2). The introduction of a rescaled time $\tau = t/V$ brings the master equation into the general form (see Appendix B)

$$\begin{aligned}&\frac{1}{V}\partial_\tau\Pi - \frac{1}{\sqrt{V}}(\nabla_{\xi}\Pi\cdot\partial_\tau\boldsymbol{\phi} - \nabla_{\eta}\Pi\cdot\partial_\tau\boldsymbol{\psi})\\ &\quad= \left(-\frac{1}{\sqrt{V}}[\boldsymbol{f}(\boldsymbol{\phi},\boldsymbol{\psi})\cdot\nabla_{\xi} + \boldsymbol{g}(\boldsymbol{\phi},\boldsymbol{\psi})\cdot\nabla_{\eta}] + \frac{\mathbf{L}}{V}\right)\Pi,\end{aligned} \tag{25}$$

where $\mathbf{L}$ is a linear operator containing various derivatives in η and ξ and $\boldsymbol{f}$ and $\boldsymbol{g}$ are functions of $\boldsymbol{\phi}$ and $\boldsymbol{\psi}$.

It is now possible to match terms on both sides of the transformed master equation (25). The order $1/\sqrt{V}$ contributions lead to

$$\begin{aligned}\frac{d}{d\tau}\phi_i &= f_i(\boldsymbol{\phi},\boldsymbol{\psi}),\\ \frac{d}{d\tau}\psi_i &= g_i(\boldsymbol{\phi},\boldsymbol{\psi}),\end{aligned} \tag{26}$$

which are just the deterministic equations for the concentrations in cell i derived in a more direct fashion earlier and given explicitly by Eq. (7). Matching the order $1/V$ contributions leads to an equation for the probability distribution Π that describes the fluctuations:

$$\partial_\tau\Pi(\boldsymbol{\xi},\boldsymbol{\eta},t) = \mathbf{L}\Pi(\boldsymbol{\xi},\boldsymbol{\eta},t). \tag{27}$$

We have analyzed the leading order result Eq. (26) in Sec. II; our aim in this section is to study the stochastic corrections given by Eq. (27). The explicit form of the operator $\mathbf{L}$ given in Appendix B shows Eq. (27) to be a Fokker-Planck equation describing a linear stochastic process. It is more convenient for our purposes to use the equivalent description of the process in terms of a linear stochastic differential equation, or Langevin equation, since this allows us to take the spatial and temporal Fourier transforms. If we carry out a Fourier transform only with respect to the spatial variable, we obtain the form [27,28]

$$\frac{\partial\tilde{\boldsymbol{\xi}}}{\partial\tau} = \tilde{\mathcal{A}}(\tilde{\boldsymbol{\xi}}) + \tilde{\boldsymbol{\mu}}(k,\tau), \tag{28}$$

where $\tilde{\boldsymbol{\mu}}(k,\tau)$ is a Gaussian noise with zero mean and correlator

$$\langle\tilde{\boldsymbol{\mu}}(k,\tau)\tilde{\boldsymbol{\mu}}^{\mathrm{T}}(k',\tau')\rangle = \tilde{\mathcal{B}}(k)\,2\pi\,\delta(k-k')\delta(\tau-\tau') \tag{29}$$

and we have introduced the convenient notation $\boldsymbol{\zeta} = (\boldsymbol{\xi},\boldsymbol{\eta})$.

The explicit forms for $\tilde{\mathcal{A}}$ and $\tilde{\mathcal{B}}$ are given in Appendix B. Since the stochastic process is linear, $\tilde{\mathcal{A}}$ is a linear function of $\tilde{\boldsymbol{\zeta}}$ and $\tilde{\mathcal{B}}$ is independent of it. Both $\tilde{\mathcal{A}}$ and $\tilde{\mathcal{B}}$ are explicit functions of τ through their dependence on the solutions of the deterministic equations $\boldsymbol{\phi}(\tau)$ and $\boldsymbol{\psi}(\tau)$. However, we are interested in fluctuations about the homogeneous state and so we evaluate these solutions in this state. In this case both $\tilde{\mathcal{A}}^*$ and $\tilde{\mathcal{B}}^*$ lose their explicit time dependence. If the noise term $\tilde{\boldsymbol{\mu}}$ is omitted from Eq. (28) [effectively by taking $\tilde{\mathcal{B}} = 0$; see Eq. (29)], then $\tilde{\boldsymbol{\zeta}}$ is nothing other than a deterministic perturbation of the deterministic dynamics. So it is not surprising that $\tilde{\mathcal{A}}^*$ is related to the elements of the Jacobian in the homogeneous state given by Eq. (19):

$$\tilde{\mathcal{A}}^*_r(k,\tau) = \sum_{s=1}^{2}\mathcal{J}^*_{rs}(k)\tilde{\zeta}_s(k,\tau). \tag{30}$$

Of course $\tilde{\mathcal{A}}$ retains an implicit dependence on time through $\tilde{\boldsymbol{\zeta}}(k,\tau)$. The form for $\tilde{\mathcal{B}}(k)$ is given by Eq. (B11). The Langevin equation (28) can now be solved by taking the temporal Fourier transform and determining the Fourier-transformed fluctuations $\tilde{\xi}(k,\omega)$ and $\tilde{\eta}(k,\omega)$ [22].

For parameter values for which the homogeneous state is stable no pattern arises in the deterministic description. However, as discussed in the Introduction, we can ask if in this region of parameters the spatial system exhibits ordered structures once fluctuations are taken into account. To probe this possible fluctuationally induced order, a useful tool is the power spectrum of the fluctuations about the homogeneous state, defined by

$$P_X(k,\omega) = \langle|\tilde{\xi}(k,\omega)|^2\rangle, \quad P_Y(k,\omega) = \langle|\tilde{\eta}(k,\omega)|^2\rangle. \tag{31}$$

In the absence of order the spectra will show an almost flat profile. If instead some type of order is present, the power spectra will typically have a characteristic peak. The position of the peak in combined (k,ω) space determines the type of structure that is present. For example, a global oscillation in time will correspond to a peak of $P(k,\omega)$ at a nonzero value of ω and at $k = 0$, whereas the power spectrum peaks at $\omega = 0$ and at a nonzero value of k for stochastic Turing patterns. As we are looking for stochastic waves we shall seek parameter values for which the power spectra display a peak at values of (k,ω) where both $k \neq 0$ and $\omega \neq 0$. The spectra are found both through simulations and analytically from the form of $\tilde{\xi}(k,\omega)$ and $\tilde{\eta}(k,\omega)$, derived from Eq. (28). The analytical calculations required to determine the power spectra are similar to those discussed in Ref. [22], but with different forms for the matrices

$\mathcal{J}^*(k)$ and $\tilde{\mathcal{B}}^*(k)$. One finds

$$P_X(\omega,k) = \frac{\mathcal{C}_X + \tilde{\mathcal{B}}^*_{11}\omega^2}{\left(\omega^2 - \Omega_0^2\right) + \Gamma^2\omega^2},$$
$$P_Y(\omega,k) = \frac{\mathcal{C}_Y + \tilde{\mathcal{B}}^*_{22}\omega^2}{\left(\omega^2 - \Omega_0^2\right) + \Gamma^2\omega^2}, \tag{32}$$

where $\Omega_0 = \sqrt{\det\mathcal{J}^*(k)}$, $\Gamma = -\mathrm{tr}\mathcal{J}^*(k)$, and $\mathcal{C}_X(k)$ and $\mathcal{C}_Y(k)$ are given in Appendix B. The expressions in Eqs. (32) constitute a full analytical characterization of the spatiotemporal power spectra of fluctuations or, equivalently, of their spatiotemporal correlation properties. This completes the mathematical analysis within the van Kampen formalism. The form of the spectra obtained and their interpretation will be discussed in the following section.

IV. RESULTS

The main purpose of this paper is to investigate how intrinsic fluctuations can bring about stochastic waves. Before we turn to the stochastic dynamics it is convenient to characterize the behavior of the nonlocal Brusselator model in the deterministic approximation. Having derived analytical expressions for the homogeneous state of the deterministic system [see Eq. (9)], as well as for the corresponding Jacobian Eq. (19), it is straightforward to obtain the stability properties of the system as a function of the model parameters. This is discussed at the end of Sec. II and in Appendix A. Given the comparatively large number of parameters, we focus on a representative selection of phase diagrams.

The properties of the deterministic dynamics at varying values of the parameters β and c (and keeping all other parameters fixed) are illustrated in Fig. 1. For a fixed value of c we find a phase at intermediate values of $\beta \in [\beta_W, \beta_T]$ in which the homogeneous state is stable against fluctuations

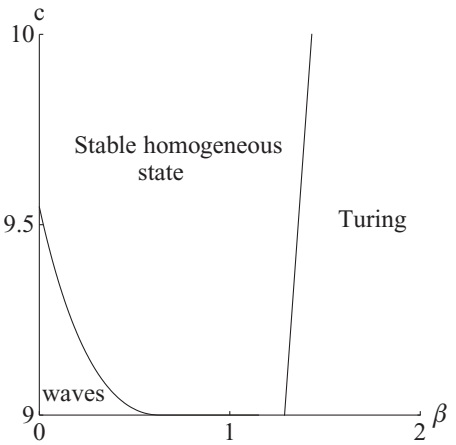

FIG. 1. Phase diagram in the (c,β) plane for the deterministic equations (7) obtained with a linear analysis of the homogeneous state Eq. (9) for $a = d = \alpha = 1$, $\sigma = 2$, and $b = 10$. The model exhibits a phase in which the homogeneous fixed point is stable, along with phases with Turing patterns and traveling waves. The two lines in the diagram, $\beta_W(c)$ and $\beta_T(c)$, indicate the onset of these instabilities. Far from these lines simultaneous instabilities may occur (e.g., traveling waves and Turing patterns).

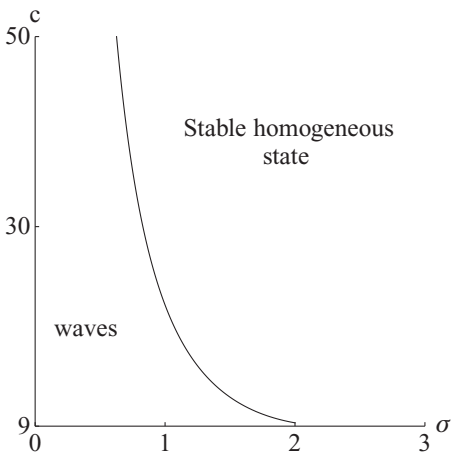

FIG. 2. Phase diagram for the deterministic dynamics, obtained from Eqs. (7) for $a = d = \alpha = 1$, $\beta = 0.1$, and $b = 10$. The solid line marks the onset of a wave instability $c = c_W(\sigma)$. The diagram illustrates the role of the nonlocal interaction in generating a wave instability.

of any wave number. At a critical value $\beta = \beta_T(c)$ a Turing instability sets in, i.e., an unstable mode occurs at a nonzero wave number, with the corresponding eigenvalue being real. At values of β lower than some second critical value $\beta_W(c)$ the instability occurs again at a nonzero wave number, but now the corresponding eigenvalue is complex, indicating a wave instability. We have thus established that the nonlocal Brusselator model exhibits Turing instabilities as well as traveling-wave instabilities in the deterministic limit.

In order to illustrate the role of the nonlocal interaction term we show a second phase diagram, now in the (σ,c) plane, in Fig. 2. Recall that the model parameter σ characterizes the range of the nonlocal interaction: For small values of σ the interaction kernel in Eqs. (7) decays slowly with distance and the interaction is therefore long range. For large σ the interaction range is small; in the limit $\sigma \to \infty$ one recovers the standard Brusselator model with purely local interactions. This is clear from Eq. (2): The only term in the sum that is independent of σ is the $j = 0$ term; all the others exponentially decay with σ and so vanish as $\sigma \to \infty$. Thus the sum tends to m_i/V as $\sigma \to \infty$.

As seen in Fig. 2, the long-range nature of the interactions can promote the occurrence of traveling waves in the deterministic system. By varying σ at a fixed value of c (and all other model parameters fixed as indicated in the caption of Fig. 2) one finds that the homogeneous state is stable at large values of σ, i.e., when interactions are localized. As σ is reduced (the interaction range is increased) a wave instability sets in.

We now turn to the stochastic system and show the spatiotemporal behavior of the concentration of Y molecules in Fig. 3. It is important to stress that we have chosen values of the model parameters such that the deterministic system has a stable homogeneous state. More specifically, for the parameters chosen in Fig. 3, the system is in the stable phase of Fig. 2, but near the line along which a wave instability occurs in the deterministic model. As demonstrated by the diagonal structures in the space-time representation of Fig. 3, the stochastic system displays traveling stochastic waves for

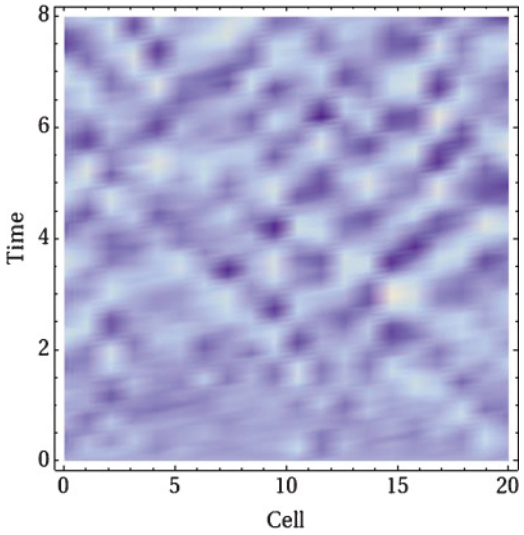

FIG. 3. (Color online) Spatiotemporal dynamics of the concentration of Y molecules in the stochastic wave regime. The number of particles, obtained from a single run of the stochastic dynamics, is reported on a scale of shades (with lighter shades indicating a larger number of Y_i particles per cell and dark shades representing low concentrations). Stochastic waves are seen as diagonal structures in the figure, representing both right-moving and left-moving waves. The system considered is a one-dimensional ring of 20 cells, each of which has a volume $V = 5000$. The parameter values are $a = d = \alpha = 1, \sigma = 2, c = b = 10$, and $\beta = 0.1$.

this choice of parameters, even if such waves are absent in the deterministic system. In order to illustrate the mechanism producing these stochastic waves we plot the dispersion relations of modes near the wave instability of the deterministic system in Fig. 4 (model parameters other than c are as in the simulations shown in Fig. 3). For $c \gtrsim 9.35$ all modes are stable and the least stable mode (i.e., the mode for which the real part of the corresponding eigenvalue is maximal among all modes) has an eigenvalue with a nonzero imaginary part and a negative real part. At $c \approx 9.35$ the wave instability

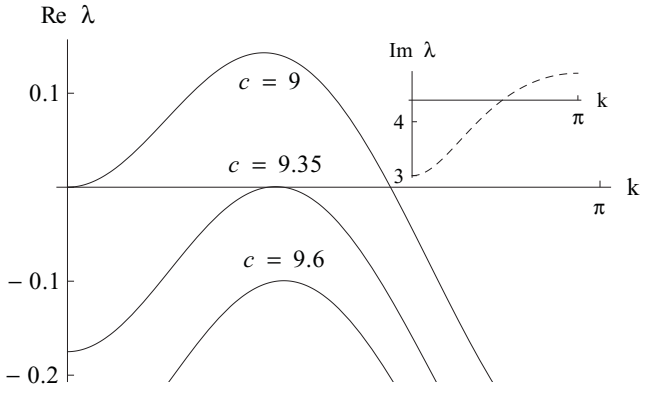

FIG. 4. Real part (solid line) and imaginary part (inset, dashed line) of $\lambda(k)$, one of the eigenvalues of the Jacobian matrix Eq. (19) (the other is its complex conjugate). The model parameters are $a = d = \alpha = 1, \sigma = 2, b = 10$, and $\beta = 0.1$. Using symmetry, we restrict the range of k to half of the Brillouin zone $[0,\pi]$. The onset of the traveling-wave instability occurs at $c \approx 9.35$.

line is crossed; one mode is now marginally stable and the corresponding eigenvalue is purely imaginary. Crucially, the instability occurs at a nonzero wave number and with a nonzero imaginary part of the corresponding eigenvalue (see inset). For $c \lesssim 9.35$ the deterministic system has unstable modes and it exhibits traveling waves.

The stochastic simulations of Fig. 3 are carried out at $c = 10$. Here all modes are stable in the deterministic system; the least stable mode has a nonzero wave number and a complex eigenvalue. In the absence of intrinsic stochasticity the system would converge to the deterministic homogeneous state. Fluctuations due to demographic noise at finite cell volumes, however, constantly cause random motion about the homogeneous state. At large but finite cell volumes, a linear approximation is in order and the fluctuations can be decomposed into their Fourier modes. The fluctuations corresponding to the least stable mode decay the slowest, on a time scale set by the real part of the corresponding eigenvalue. This effect conspires with fluctuations persistently occurring due to the mechanism now known as coherent stochastic amplification [19]. Modes that are stable in the deterministic model can effectively be excited by random fluctuations and are observed with sizable amplitude in the stochastic system. In our model this amplitude scales as $V^{-1/2}$ in the cell volume, but the prefactor multiplying this factor can be significant, resulting in stochastic waves with appreciable amplitude even at large cell volumes.

To illustrate the occurrence of stochastic waves further, we show a time series of the (re-scaled) concentration of Y molecules in a fixed cell in the top panel of Fig. 5. Coherent stochastic oscillations are clearly visible; their amplitude is seen to scale as $V^{-1/2}$ with the cell volume. Plotting the time

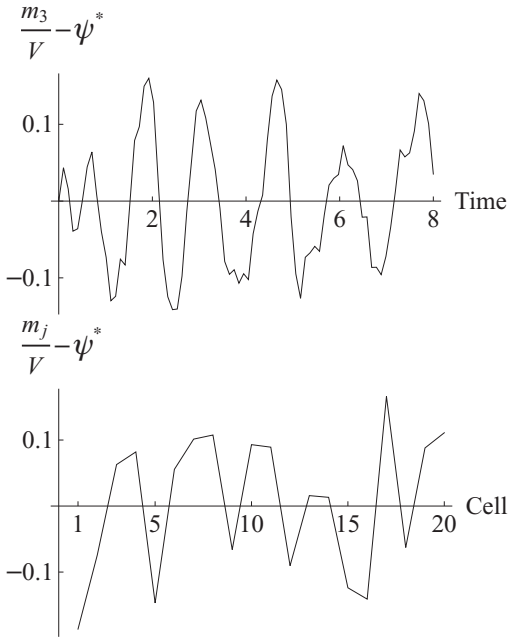

FIG. 5. Top panel: Temporal evolution of the Y concentration in a selected cell in the stochastic wave regime. Data are obtained from one run of the stochastic dynamics, with the parameter values as in Fig. 3. Bottom panel: Snapshot of the concentration of Y molecules as a function of position at a fixed time t.

series of the Y concentration in one cell, we have effectively disregarded the spatial structure of the system and focused instead on the temporal dynamics only. In this sense the top panel of Fig. 5 is similar to observations of amplified stochastic oscillations in the time series of nonspatial systems (see, for example, Ref. [19]). The bottom panel of Fig. 5 shows the concentration of Y molecules as a function of position at a fixed time. Spatial modulations, again with an amplitude scaling as $V^{-1/2}$, are seen, even though of a lower coherence than the temporal oscillations shown in the top panel. In this bottom panel we have effectively disregarded the temporal dynamics of the system and have instead focused on its spatial character. The modulations of the concentration of Y molecules as a function of position therefore constitutes the analog of stochastically driven Turing patterns reported in Refs. [4–6]. The difference between our model and those proposed previously is that it combines the spatial and the temporal aspect; the stochastic waves seen in the nonlocal Brusselator model are noise-driven patterns with structure both as a function of position and as a function of time.

The theory developed in Sec. III allows us to characterize the observed stochastic waves further. Based on the results of Eqs. (32), we are able to predict the power spectra of

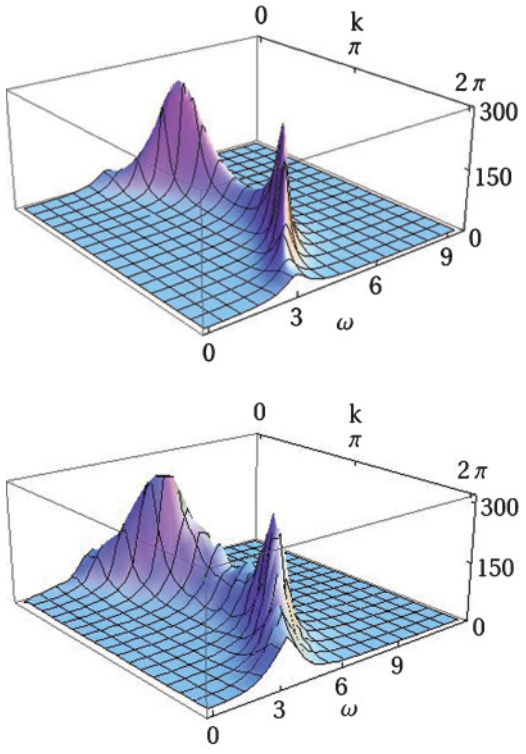

FIG. 6. (Color online) Power spectrum of the fluctuations of the Y species obtained analytically (top panel) from Eq. (32) and numerically (bottom panel) by simulating the stochastic process using the Gillespie algorithm. The agreement between the two power spectra is clearly very good. The system is in the stochastic wave regime with $a = d = \alpha = 1$, $\sigma = 2$, $c = b = 10$, and $\beta = 0.05$. The spectra show a peaked profile, which corresponds to spatiotemporal organization despite the deterministic prediction of a stable homogeneous state. The numerical spectrum is obtained by averaging 200 realizations of a finite system of 28 cells, each of which has a volume $V = 1500$.

spatiotemporal fluctuations about the homogeneous state for any choice of model parameters. Stochastic waves are to be expected whenever the highest peak of these power spectra is found simultaneously at a nonzero wave number k (indicating a nontrivial spatial structure) and at a nonzero angular frequency ω (indicating a complex eigenvalue and hence oscillatory behavior as a function of time). An example of a power spectrum with these properties, obtained from the theory of Sec. III, is shown in the top panel of Fig. 6; for comparison we show measurements from direct numerical simulations in the bottom panel. As seen from this figure, the agreement between theory and simulations is excellent.

V. CONCLUSION

This paper has been concerned with the investigation of stochastic effects in a nonlocal extension of the Brusselator model. An analysis of this model on the deterministic level reveals that nonlocal interactions can promote the occurrence of traveling-wave instabilities, similar to what has been seen before in other chemical reaction models with long-range interactions [8]. As the main result of our work we show that the nonlocal Brusselator model can also exhibit traveling waves driven by internal fluctuations in parameter regimes in which the deterministic system converges to a homogeneous state. Based on a stochastic formulation of the model in terms of a chemical master equation and a subsequent expansion in the inverse system size, we derived analytical expressions for the power spectra of these spatiotemporal patterns, in excellent agreement with direct numerical simulations.

These findings extend previous results on noise-driven instabilities. In Ref. [19] nonspatial systems were considered and it was shown that intrinsic fluctuations can generate coherent stochastic oscillations for parameters for which the deterministic system spirals into a fixed point. The work of Refs. [4–6] instead focused on spatial systems and it was shown that intrinsic noise can generate stochastic Turing patterns, i.e., spatial structures with a constant amplitude in time. Our model combines both aspects and produces stochastic patterns with a full spatiotemporal dynamics.

These stochastic waves are seen in the power spectra of fluctuations, computed from the theoretical approach, as isolated peaks at nonzero wave number and nonzero angular frequency. While in the past it has been rather difficult to observe spatial stochastic patterns directly and most of the previous work was limited to an indirect identification in Fourier space, we have also been able to obtain direct visual confirmation of the stochastic waves in the Brusselator model with nonlocal interaction. Criteria that distinguish stochastic cycles or stochastic patterns from their deterministic analogs (limit cycles and Turing-like patterns) have been proposed [4,7,29]. However, these are not applicable to systems with nonlocal interactions of the type we have considered here due to the extra k dependence that comes about because of the nonlocality. It would be interesting to devise criteria that encompass nonlocal models as well.

The purpose of the current work is to illustrate a generic phenomenon that is expected to occur in a wide class of systems; the Brusselator model was chosen to illustrate the basic idea because it is simple and widely studied. The effects

of noise on traveling waves has been investigated in the past, but most of these studies depended on the properties of the specific system under consideration. For example, a simple reaction-diffusion equation displaying traveling waves is the Fisher equation [30]. For this system it is known that noise may alter the properties of the waves (see, for instance, Ref. [31]) and may also be responsible for the emergence of noise-driven traveling waves [32]. However, these waves are different from those we have discussed here, as they do not arise from an underlying unstable homogeneous state. A related point is that the Fisher equation has only one species, whereas we need at least two interacting species since we require complex eigenvalues to trigger the wave instability [2].

We expect that the mechanism of coherent amplification applies to more complicated linear instabilities as well [2] and that the concept of stochastic waves is relevant in other models with traveling fronts. We also expect that the analytical formalism we have developed here for spatial systems with nonlocal interaction can successfully be employed to study broader classes of individual-based models. This may include models of the spread of epidemics, in which infection can occur at a distance; deterministic models of such processes have been considered [33,34]. As stochastic patterns are found in more and more model systems, we expect the search for them in real systems to intensify and the understanding of the underlying causes of pattern formation in physical, biological, and social systems to broaden.

ACKNOWLEDGMENTS

T.B. wishes to thank the EPSRC for partial support and T.G. acknowledges support from the Research Councils UK (reference No. EP/E500048/1).

APPENDIX A: TURING AND WAVE INSTABILITIES

In this appendix we derive the conditions that allow the onset of Turing or wave instabilities to be located. Such criteria exist in the literature [1–3], but most of them rely on the standard reaction-diffusion paradigm and will not be applicable in our case, which includes a nonlocal kernel and thus an extra k dependence over and above that coming from the diffusion terms. We need therefore a more general approach, described below, which closely follows Ref. [35].

We start by defining the region of parameter space in which the homogeneous state is stable. Its borders delimit the instabilities whose type can be determined from the analysis below. The stability condition $\mathrm{Re}[\lambda_i(k)] < 0$ for all k can be conveniently rewritten using the trace and determinant if the Jacobian is a 2×2 matrix as

$$\det\mathcal{J}^*(k) > 0, \quad \mathrm{tr}\mathcal{J}^*(k) < 0 \quad \forall k. \tag{A1}$$

The stability region is the set of parameters in which the above inequalities hold. By plotting $\det\mathcal{J}^*(k)$ against $\mathrm{tr}\mathcal{J}^*(k)$ we see that we may leave the stability region by violating one of these inequalities, that is, (i) when there exists a $k_C \neq 0$ such that $\det\mathcal{J}^*(k_C) = 0$ whereas $\mathrm{tr}\mathcal{J}^*(k) < 0\ \forall k$ or (ii) there exists a $k_C \neq 0$ such that $\mathrm{tr}\mathcal{J}^*(k_C) = 0$ whereas $\det\mathcal{J}^*(k) > 0\ \forall k$. It is also possible that the determinant and trace become simultaneously zero, but this is a degenerate case, which we do not consider here.

Now recall that the eigenvalues of the Jacobian are given by

$$\lambda_{1,2} = \tfrac{1}{2}[\mathrm{tr}\mathcal{J}^* \pm \sqrt{(\mathrm{tr}\mathcal{J}^*)^2 - 4\det\mathcal{J}^*}], \tag{A2}$$

from which the imaginary part of the eigenvalues may be found. From the discussion at the end of Sec. II we can see that the above conditions defining the boundaries of the stability region correspond respectively to a Turing instability (case (i) above) and to a wave instability (case (ii) above).

The stability conditions as given are not so convenient to deal with directly because of the presence of inequalities that must be solved for every k. To overcome this we suppose that $\mathrm{tr}\mathcal{J}^*(k)$ has a global maximum at k_M and $\det\mathcal{J}^*(k)$ has a global minimum at k_m, a hypothesis that will be discussed further below. In this case the two conditions may be rewritten as $\det\mathcal{J}^*(k_m) = 0$ and $\mathrm{tr}\mathcal{J}^*(k_M) < 0$ (Turing instability) and $\mathrm{tr}\mathcal{J}^*(k_M) = 0$ and $\det\mathcal{J}^*(k_m) > 0$ (wave instability). These are the conditions we have used to obtain Figs. 1 and 2.

We can now check that the specific forms of $\mathrm{tr}\mathcal{J}^*(k)$ and $\det\mathcal{J}^*(k)$ in our model have the required extrema. Finding the extremal points of $\mathrm{tr}\mathcal{J}^*(k_M)$ can easily be achieved analytically; for $\det\mathcal{J}^*(k_m)$ it is a little more difficult. However, checking the existence of a global maximum or minimum numerically is straightforward and we have verified that for the range of parameters of interest to us in this paper such extrema always exist and moreover give the boundaries shown in Figs. 1 and 2.

APPENDIX B: THE VAN KAMPEN SYSTEM-SIZE EXPANSION

A description of the general structure and methodology behind the system-size expansion, as applied to the system under consideration, is given in Sec. III. In this appendix we give some of the technical details that would otherwise disrupt the flow of the arguments in the main text.

The application of the method is facilitated by writing down the master equation (5) in terms of the step operators Eqs. (20). An example is given in Eq. (21) for the first reaction of the set of reactions given by Eqs. (1). When all eight reactions are included the master equation is given by

$$\begin{aligned}
\frac{d}{dt}P_{\mathbf{n},\mathbf{m}}(t) &= \sum_{i=-\infty}^{\infty}\Big((\epsilon^-_{X,i}-1)T(n_i+1,m_i|n_i,m_i) \\
&+(\epsilon^+_{X,i}-1)T(n_i-1,m_i,|n_i,m_i) \\
&+(\epsilon^+_{X,i}\epsilon^-_{Y,i}-1)T(n_i-1,m_i+1|n_i,m_i) \\
&+(\epsilon^-_{X,i}\epsilon^+_{Y,i}-1)T(n_i+1,m_i-1|n_i,m_i) \\
&+\sum_{j\in\{i-1,i+1\}}[(\epsilon^+_{X,i}\epsilon^-_{X,j}-1)\,T(n_i-1,n_j+1|n_i,n_j) \\
&+(\epsilon^+_{X,j}\epsilon^-_{X,i}-1)T(n_i+1,n_j-1|n_i,n_j) \\
&+(\epsilon^+_{Y,j}\epsilon^-_{Y,i}-1)T(m_i+1,m_j-1|m_i,m_j) \\
&+(\epsilon^+_{Y,i}\epsilon^-_{Y,j}-1)T(m_i-1,m_j+1|m_i,m_j)]\Big) \\
&\times P_{\mathbf{n},\mathbf{m}}(t).
\end{aligned} \tag{B1}$$

The fundamental ansatz of the system-size expansion is given by Eq. (22) in the main text. It leads to the expression Eq. (24) for the left-hand side of the master equation. The right-hand side can be evaluated by observing that the step operators Eqs. (20) can be expanded in the inverse of the square root of the system size $V^{-1/2}$, giving rise to the following expressions [16]:

$$\epsilon^{\pm}_{X,i} \approx 1 \pm \frac{1}{\sqrt{V}}\partial_{\xi_i} + \frac{1}{2V}\partial^2_{\xi_i}, \quad \epsilon^{\pm}_{Y,i} \approx 1 \pm \frac{1}{\sqrt{V}}\partial_{\eta_i} + \frac{1}{2V}\partial^2_{\eta_i}. \tag{B2}$$

This, together with the substitution of the ansatz Eqs. (22) into the transition rates Eqs. (2) and the replacement of $P_{\mathbf{n},\mathbf{m}}(t)$ by $\Pi(\boldsymbol{\xi},\boldsymbol{\eta},t)$, allows us to expand the right-hand side in powers of $V^{-1/2}$.

Equating the left- and right-hand sides of the master equation gives the general form

$$\begin{aligned}&\partial_t \Pi - \sqrt{V}\,\nabla_{\boldsymbol{\xi}}\Pi\cdot\partial_t\boldsymbol{\phi} - \sqrt{V}\,\nabla_{\boldsymbol{\eta}}\Pi\cdot\partial_t\boldsymbol{\psi}\\ &\quad= \left(-\frac{1}{\sqrt{V}}[\boldsymbol{f}(\boldsymbol{\phi},\boldsymbol{\psi})\cdot\nabla_{\boldsymbol{\xi}} + \boldsymbol{g}(\boldsymbol{\phi},\boldsymbol{\psi})\cdot\nabla_{\boldsymbol{\eta}}] + \frac{\mathbf{L}}{V}\right)\Pi,\end{aligned} \tag{B3}$$

where $\mathbf{L}$ is a linear operator containing various derivatives in η and ξ and $\boldsymbol{f}$ and $\boldsymbol{g}$ are functions of $\boldsymbol{\phi}$ and $\boldsymbol{\psi}$. After the introduction of a rescaled time $\tau = t/V$, Eq. (25) is obtained. This is now in a form where the various terms on both sides of the equation can be balanced.

Equating the leading-order terms in Eq. (25) gives equations whose general structure is displayed in Eqs. (26) and whose specific form is in Eqs. (7). Equating the next-to-leading-order terms gives an equation with a general structure Eq. (27) and specific form

$$\begin{aligned}\partial_\tau\Pi = \sum_{i=-\infty}^{\infty}\Bigg(&-\sum_{r=1}^{2}\partial_{\zeta_{r,i}}(\mathcal{A}_{r,i}\Pi)\\ &+\frac{1}{2}\sum_{r,s=1}^{2}\sum_{j=i-1}^{i+1}\partial_{\zeta_{s,i}}\partial_{\zeta_{r,j}}[\mathcal{B}_{rs,ij}\Pi]\Bigg),\end{aligned} \tag{B4}$$

where for convenience we have introduced the notation $\zeta_1 \equiv \xi$ and $\zeta_2 \equiv \eta$. The precise forms of $\mathcal{A}_{r,i}$ and $\mathcal{B}_{rs,ij}$ will be discussed below, but as mentioned in the main text it is easier for our purposes to work with the equivalent Langevin equation [27,28]

$$\frac{d\boldsymbol{\zeta}_i}{d\tau} = \mathcal{A}_i(\boldsymbol{\zeta}) + \boldsymbol{\mu}_i(\tau), \tag{B5}$$

where $\boldsymbol{\mu}_i$ is a Gaussian noise with zero mean and correlator

$$\left\langle \boldsymbol{\mu}_i(\tau)\boldsymbol{\mu}_j^{\mathrm{T}}(\tau')\right\rangle = \mathcal{B}_{ij}\,\delta(\tau-\tau'). \tag{B6}$$

We are then able to take the Fourier transform of this equation in both space and time to give Eq. (28).

The Langevin equation (28) is defined by two contributions: the drift term and the diffusion matrix. Since the drift term is related to the Jacobian of the system, as presented in Eq. (30), we will give only the expression for the diffusion matrix.

The diffusion matrix $\mathcal{B}$ has elements $\mathcal{B}_{rs,ij}$, where r and s index the species and i and j the cell. In the following the expressions are given for each r and s and for a given cell i. The only nonzero values of $\mathcal{B}_{rs,ij}$ occur when $j = i-1, i$, or $i+1$, which are given respectively as the first, second, and third entries of a row vector:

$$\begin{aligned}\mathcal{B}_{11,i} = \Bigg(&-\alpha(\phi_i+\phi_{i-1}),\ a+(b+d)\phi_i\\ &+c\Lambda\sum_{j=-\infty}^{\infty}e^{-\sigma|j|}\phi_i^2\psi_{i-j}+\alpha(\phi_{i-1}+2\phi_i+\phi_{i+1}),\\ &-\alpha(\phi_i+\phi_{i+1})\Bigg),\\ \mathcal{B}_{12,i} = \mathcal{B}_{21,i} = \Bigg(&0,\ -b\phi_i - c\Lambda\sum_{j=-\infty}^{\infty}e^{-\sigma|j|}\phi_i^2\psi_{i-j},0\Bigg),\\ \mathcal{B}_{22,i} = \Bigg(&-\beta(\psi_i+\psi_{i-1}),\ b\phi_i+c\Lambda\sum_{j=-\infty}^{\infty}e^{-\sigma|j|}\phi_i^2\psi_{i-j}\\ &+\beta(\psi_{i-1}+2\psi_i+\psi_{i+1}),\ -\beta(\psi_i+\psi_{i+1})\Bigg).\end{aligned} \tag{B7}$$

Evaluating them in the homogeneous state gives

$$\begin{aligned}\mathcal{B}^*_{11,i} &= \left[-\frac{2a\alpha}{d},\ 2a+\frac{2ab}{d}+\frac{4a\alpha}{d},\ -\frac{2a\alpha}{d}\right],\\ \mathcal{B}^*_{12,i} &= \mathcal{B}^*_{21,i} = \left[0,\ -\frac{2ab}{d},0\right],\\ \mathcal{B}^*_{22,i} &= \left[-\frac{2bd\beta}{ac},\ \frac{2ab}{d}+\frac{4bd\beta}{ac},\ -\frac{2bd\beta}{ac}\right].\end{aligned} \tag{B8}$$

The structure of $\mathcal{B}^*_{rs,ij}$ can be seen from Eqs. (B8) to be

$$\mathcal{B}^*_{rs,ij} = b^{(0)}_{rs}\delta_{i-j,0} + b^{(1)}_{rs}\delta_{|i-j|,1}, \tag{B9}$$

where the two matrices $b^{(0)}$ and $b^{(1)}$ can be read off from Eqs. (B8). It is then straightforward [22] to calculate the spatial Fourier transform $\tilde{\mathcal{B}}_{rs} \equiv \tilde{\mathcal{B}}_{rs}(k)$ of the matrices Eqs. (B8) with respect to the variable $i-j$:

$$\tilde{\mathcal{B}}^*_{rs}(k) = \left(b^{(0)}_{rs} + 2b^{(1)}_{rs}\right) + b^{(1)}_{rs}\tilde{\Delta}, \tag{B10}$$

where $\tilde{\Delta}$ is given by Eq. (17). The explicit forms are

$$\begin{aligned}\tilde{\mathcal{B}}^*_{11}(k) &= \frac{2a}{d}(b+d) - \frac{2a\alpha}{d}\tilde{\Delta},\\ \tilde{\mathcal{B}}^*_{12}(k) &= \tilde{\mathcal{B}}^*_{21}(k) = -\frac{2ab}{d},\\ \tilde{\mathcal{B}}^*_{22}(k) &= \frac{2ab}{d} - \frac{2bd\beta}{ac}\tilde{\Delta}.\end{aligned} \tag{B11}$$

The power spectra of the stochastic oscillations, defined by Eqs. (31), have the form of Eqs. (32). The functions $\mathcal{C}_X$ and $\mathcal{C}_Y$ are defined by

$$\begin{aligned}\mathcal{C}_X(k) &= \tilde{\mathcal{B}}^*_{11}(k)\mathcal{J}^*_{22}(k)^2 - 2\tilde{\mathcal{B}}^*_{12}(k)\mathcal{J}^*_{12}(k)\mathcal{J}^*_{22}(k)\\ &\quad+\tilde{\mathcal{B}}^*_{22}(k)\mathcal{J}^*_{12}(k)^2,\\ \mathcal{C}_Y(k) &= \tilde{\mathcal{B}}^*_{22}(k)\mathcal{J}^*_{11}(k)^2 - 2\tilde{\mathcal{B}}^*_{12}(k)\mathcal{J}^*_{21}(k)\mathcal{J}^*_{11}(k)\\ &\quad+\tilde{\mathcal{B}}^*_{11}(k)\mathcal{J}^*_{21}(k)^2.\end{aligned} \tag{B12}$$

[1] A. M. Turing, Philos. Trans. R. Soc. London B **237**, 37 (1952).

[2] M. C. Cross and H. S. Greenside, *Pattern Formation and Dynamics in Non-Equilibrium Systems* (Cambridge University Press, Cambridge, 2009).

[3] J. D. Murray, *Mathematical Biology Vol. II* (Springer-Verlag, Berlin, 1993).

[4] T. Butler and N. Goldenfeld, Phys. Rev. E **80**, 030902(R) (2009).

[5] T. Biancalani, D. Fanelli, and F. Di Patti, Phys. Rev. E **81**, 046215 (2010).

[6] M. Scott, F. J. Poulin, and H. Tang, Proc. R. Soc. London Ser. A **467**, 718 (2011).

[7] T. Butler and N. Goldenfeld, Phys. Rev. E **84**, 011112 (2011).

[8] E. M. Nicola, M. Bär, and H. Engel, Phys. Rev. E **73**, 066225 (2006).

[9] A. N. Zaikin and A. M. Zhabotinsky, Nature (London) **225**, 535 (1970).

[10] *Oscillations and Traveling Waves in Chemical Systems*, edited by R. J. Field and M. Burger (Wiley Interscience, New York, 1985).

[11] Z. Noszticzius, W. Horsthemke, W. D. McCormick, H. L. Swinney, and W. Y. Tam, Nature (London) **329**, 619 (1987).

[12] M. P. Hassell, H. N. Comins, and R. M. May, Nature (London) **353**, 255 (1991).

[13] E. Ranta and V. Kaitala, Nature (London) **390**, 456 (1997).

[14] B. T. Grenfell, O. N. Bjørnstad, and J. Kappey, Nature (London) **414**, 716 (2001).

[15] D. A. T. Cummings, R. A. Irizarry, N. E. Huang, T. P. Endy, A. Nisalak, K. Ungchusak, and D. S. Burke, Nature (London) **427**, 344 (2004).

[16] N. G. van Kampen, *Stochastic Processes in Physics and Chemistry*, 3rd ed. (Elsevier Science, Amsterdam, 2007).

[17] D. Alonso, A. J. McKane, and M. Pascual, J. R. Soc. Interface **4**, 575 (2007).

[18] G. Rozhnova and A. Nunes, Phys. Rev. E **79**, 041922 (2009).

[19] A. J. McKane and T. J. Newman, Phys. Rev. Lett. **94**, 218102 (2005).

[20] A. Traulsen, J. C. Claussen, and C. Hauert, Phys. Rev. Lett. **95**, 238701 (2005).

[21] C. Castellano, S. Fortunato, and V. Loreto, Rev. Mod. Phys. **81**, 591 (2009).

[22] C. A. Lugo and A. J. McKane, Phys. Rev. E **78**, 051911 (2008).

[23] D. T. Gillespie, J. Comput. Phys. **22**, 403 (1976).

[24] D. T. Gillespie, J. Phys. Chem. **81**, 2340 (1977).

[25] P. Glansdorff and I. Prigogine, *Thermodynamic Theory of Structure, Stability and Fluctuations* (Wiley Interscience, Chichester, 1971).

[26] R. P. Boland, T. Galla, and A. J. McKane, Phys. Rev. E **79**, 051131 (2009).

[27] C. W. Gardiner, *Handbook of Stochastic Methods for Physics, Chemistry and the Natural Sciences*, 4th ed. (Springer, New York, 2009).

[28] H. Risken, *The Fokker-Planck Equation—Methods of Solution and Applications*, 2nd ed. (Springer, Berlin, 1989).

[29] M. Pineda-Krch, H. J. Blok, U. Dieckmann, and M. Doebeli, Oikos **116**, 53 (2007).

[30] R. A. Fisher, Ann. Eugen. **7**, 355 (1937).

[31] E. Moro, Phys. Rev. Lett. **87**, 238303 (2001).

[32] O. Hallatschek, PLoS Comput. Biol. **7**, e1002005 (2011).

[33] M. J. Keeling and P. Rohani, *Modeling Infectious Diseases in Humans and Animals* (Princeton University Press, Princeton, 2008).

[34] Z.-C. Wang and J. Wu, Proc. R. Soc. London Ser. A **466**, 237 (2010).

[35] E. M. Nicola, Ph.D. thesis, University of Dresden, 2001.